Scale-dependent erosional patterns in steady and transient state landscapes

Alejandro Tejedor[1], Arvind Singh[2], Ilya Zaliapin[3], Alexander L. Densmore[4], Efi Foufoula-Georgiou[1,5]

[1]Department of Civil and Environmental Engineering, University of California, Irvine, Irvine, California, USA

[2]Department of Civil, Environmental and Construction Engineering, University of Central Florida, Orlando, Florida, USA

[3]Department of Mathematics and Statistics, University of Nevada, Reno, Reno, Nevada, USA

[4]Department of Geography and Institute of Hazard, Risk, and Resilience, Durham University, Durham DH1 3LE, UK

[5]St. Anthony Falls Laboratory and National Center for Earth-Surface Dynamics, University of Minnesota, Minneapolis, Minnesota, USA

Abstract

Landscape topography is the expression of the dynamic equilibrium between external forcings (e.g. climate and tectonics) and the underlying lithology. The magnitude and spatial arrangement of erosional and depositional fluxes dictate the evolution of landforms during both statistical steady state (SS) and transient states (TS) of major landscape reorganization. For SS landscapes, the common expectation is that any point of the landscape has equal chance to erode at below or above the landscape median erosion rate. We show here that this is not the case. Afforded by a unique experimental landscape that provided a detailed space-time recording of erosional fluxes, and by defining the so-called "E50-area curve", we reveal for the first time that there exists a hierarchical pattern of erosion. Specifically, hillslopes and fluvial channels erode more rapidly than the landscape median rate while intervening parts of the landscape in terms of upstream contributing areas (colluvial regime) erode more slowly. We explain this apparent paradox by documenting the dynamic nature of SS landscapes – landscape locations through time may transition from being a hillslope to a valley and then to a fluvial channel due to ridge migration, channel piracy and small-scale landscape dynamics. Under TS conditions caused by increased precipitation, we show that the E50-area curve changes shape drastically during landscape reorganization. Scale-dependent erosional patterns as observed in this study suggest benchmarks in evaluating numerical models and interpreting the variability of sampled erosional rates in field landscapes.

Introduction

Landscape topography is sculpted via material fluxes that are controlled by the interplay of different external forcings, such as climate and tectonics, with the underlying lithology (1-6). Landscapes evolving under constant external forcings tend to achieve steady state (SS) configurations where the material flux provided by rock uplift relative to baselevel is balanced by erosion. These landscapes can be subdivided into different geomorphic process regimes, such as hillslopes, colluvial channels, and fluvial channels, typically on the basis of variables such as topographic gradient and the upstream contributing area that concentrates runoff (7). Whether the flux balance occurs across all of these regimes and at all spatial scales (even pointwise), or is only applicable to the total or bulk fluxes at the landscape scale has unavoidable consequences for the dynamic character of the landscape (8); the former situation leads to time-invariant (frozen) landforms, while the latter allows for a dynamic component of SS landscapes. While many numerical landscape evolution models result in *static* SS landscapes under simple boundary conditions (usually vertical uplift and uniform rainfall) (9-14), physical experiments consistently produce SS landscapes with dynamic landforms (15-18). This notion of dynamic SS landscapes, where drainage divides continuously migrate and local erosion rates are therefore time-variant and spatially non-uniform, is also supported by field and low-temperature thermochronological evidence (19-21). Dynamic landscape behavior has been successfully incorporated into some numerical models by various mechanisms such as landsliding (22), the use of more realistic flow-routing algorithms (23), or via hillslope-fluvial process interactions (24).

If erosion rates vary in space and time, how can one distinguish steady state (SS) landscapes from transient state (TS) landscapes, which respond to a change in external forcings? One approach would be to compare the variability in erosion rates of SS landscapes, both in terms of their magnitudes and spatial distribution, with those under TS conditions. Despite good knowledge of how individual landscape components, such as alluvial rivers, bedrock rivers, or hillslopes (25-29), respond to change in external forcing, our understanding of the organized erosional response of the landscape as a whole remains elusive. Recent studies have tried to explain the variability of erosion rates in natural landscapes, due for example to stochasticity of hillslope processes or knickpoint dynamics (21,30-32). However, a comprehensive characterization of such variability, especially in terms of spatial patterns, would demand repeated topographic data at high spatial resolution and over long periods of time. Such data are typically not available for natural landscapes, making physical experiments (15-18,27,33,34) a necessary tool for exploring erosion variability. While physical experiments have been used to document large-scale TS landscape responses (15-18, 27), they have not typically been utilized to examine the multiscale spatial variability of sediment fluxes within SS conditions to quantify the dynamic nature of SS landscapes and to compare with TS responses.

In this paper, we analyze a unique experimental landscape, which provides a detailed space-time record of the topography produced at the eXperimental Landscape Evolution (XLE) facility at St. Anthony Falls Laboratory (17). We seek to (i) fully characterize SS landscapes in terms of local sediment fluxes to advance our understanding of their dynamic nature, and (ii) quantify the manner in which landscapes reorganize in response to changes in external forcing.

Brief description of the experimental setup

The eXperimental Landscape Evolution (XLE) facility (see Fig. 1 for schematic) consists of an erosion box (0.5 x 0.5 x 0.3 m^3) with two main controlling variables: (i) *uplift rate*, adjusted by lowering two opposing sides mimicking mountain uplift, and (ii) *rainfall intensity*, simulated using 20 ultrafine misting nozzles (droplet size <10 μm) to achieve approximate spatial uniformity over the box. The rainfall droplet size was small enough to avoid splash disturbances by the drop impact on the landscape surface. The sediment used in the experiment was a homogeneous mixture of fine silica (D_{50} = 25 μm) with ~35% water content by volume. The facility was equipped with a high-resolution laser scanner that was able to obtain the topographic elevation $h(x,y,t)$ of the whole surface in 5 seconds at a spatial resolution of 0.5 mm and a vertical accuracy of better than 0.5 mm. For this experiment, topographic data were acquired every 5 minutes. We refer to *Singh et al.* (17) for a comprehensive discussion of the experimental setup and collected data.

Steady State Landscape

Assuming uniform grain size distribution and material porosity, as is the case in our experiment, the pixel-wise measured topographic change $\left(\frac{\partial h_i}{\partial t}\right)$ relates to the flux divergence $\nabla \cdot \vec{q}_{s,i}$ and the constant uplift rate U by the Exner equation:

$$\frac{\partial h_i}{\partial t} = U - \nabla \cdot \vec{q}_{s,i} \qquad (1)$$

The erosion depth (ED) at pixel i over a time interval [t, $t+\Delta t$] is obtained by integrating the flux divergence:

$$ED_i\left(t,\Delta t\right) = \int_{t}^{t+\Delta t} \nabla \cdot \vec{q}_{s,i}(t)dt \qquad (2)$$

where positive (negative) values of ED_i imply net erosion (deposition) at pixel i.

A landscape is said to be at SS when the erosional fluxes balance out the sediment flux provided by the rock uplift. Depending on the scale at which this flux balance is applicable, two different types of SS can be defined (8). In *flux* SS, the total flux of sediment leaving the system balances the amount provided by tectonic uplift during an interval of time Δt:

$$\text{SS:} \quad \left\langle ED_i^{SS}\left(t,\Delta t\right)\right\rangle = \left\langle ED_i^{SS}\left(\Delta t\right)\right\rangle = U \cdot \Delta t \qquad (3)$$

where $\langle \cdot \rangle$ denotes spatial average over all pixels *i* and the first equality acknowledges the time-independent average flux. Flux SS is also referred as *statistical* SS, acknowledging that several statistical properties of the landscape such as slope and upstream contributing area probability distributions, sediment discharge or river network properties, remain constant (17,18). In *topographic* SS, the surface elevation does not change over time because the divergence of sediment flux is the same at every point of the landscape and is exactly equal to the uplift rate:

$$\frac{\partial h_i}{\partial t} = 0; \qquad U = \nabla \cdot \vec{q}_{s,i} \qquad \forall i \qquad (4)$$

Using the XLE facility, we let the landscape evolve to a statistical SS with constant uplift rate U = 20 mm/h and constant precipitation rate P = 45 mm/h for 8 hours. SS conditions were inferred by a time-invariant sediment flux rate equal to the uplift rate (17). Fig. 2 illustrates the SS nature of the landscape by showing the time invariance of two important statistical properties: the slope-area curve (Fig. 2A), and the probability distribution of pixel-wise erosion depths, which also confirms a constant mean erosion depth (Fig. 2B). The slope-area curves were obtained from four consecutive topographies at SS (measured 5 min apart) using the steepest downslope direction to estimate local slope and the D-infinity algorithm (36,37) to compute upstream contributing areas. Slope-area curves are a useful tool to reveal the scales of geomorphic organization (7,38-45). From changes in the trends of these curves we can differentiate three process regimes: hillslopes, draining upstream contributing areas that range from 1 to approximately 10 pixels, or up to 2.5 mm^2; a colluvial regime corresponding to intermediate upstream contributing areas of 2.5 to 250 mm^2; and a fluvial regime corresponding to upstream contributing areas larger than 250 mm^2. The specific values are obtained via analysis of slope increments and detection of change of trends as discussed in *Singh et al.* (17). The overlap of consecutive slope-area curves derived from different topographies at SS shows that there was no significant change in these regimes and thus no structural reorganization of the landscape. Notice that the higher variability observed for large upstream contributing areas is due to the smaller sample size available to compute the corresponding slope. We also computed probability density functions (PDFs) of the pixel-wise erosion depth, with positive values indicating erosion and negative values deposition, computed by taking differences of elevation of consecutive topographies measured 5 min apart. From the overlapping distributions and from the results of a Kruskal-Wallis test (46), we conclude that the PDFs are statistically indistinguishable, revealing the statistical SS nature of erosional and depositional processes. We also note that the shape of the PDFs reveals that the landscape is not frozen (that is, it is not a topographic SS); if it were, the PDF would be just a Dirac delta function (single value) centered at the value of the uplift depth ($U \cdot \Delta t$ - i.e. depth of material provided by the uplift in Δt =5 min). The observed complex distribution of local erosion depths raises the question about the spatial distribution of the variability in the erosion magnitude. In the next section we unveil, via a spatial analysis of the sediment fluxes, a stationary *scale*-dependent pattern of erosion for SS landscapes.

Scale*-dependent (or hierarchical) erosional patterns: the *E50-area curve

We ask whether there exists a characteristic erosional signature of steady state landscapes reflective of their geomorphologic organization. For that we interrogate the landscape in terms of the pixel-wise erosion (deposition) depth as a function of the pixel location parameterized by the upstream contributing area. Specifically, we compute the probability density function of erosion depth for sets of pixels grouped in 100 equal probability area bins according to their upstream drainage area A_i. We summarize the results of this analysis in a so-called "E50-area curve" (Fig. 3A), where we estimate the probability that the pixel-wise erosion depth within each drainage area bin exceeds the median erosion depth of the whole landscape. We highlight two main points revealed by the E50-area curves. First, the stationary shape of the curve for fluxes computed at different SS intervals reveals a statistical pattern that is persistent over time; that is, the E50-area curve is a statistical signature of the steady state landscape.

Second, the curves have a characteristic non-linear shape that deviates from the trivial horizontal curve (equal to 0.5 for all values of upstream contributing area) that would be expected under topographic SS. Specifically, the E50-area curve reveals that the regimes of the landscapes characterized by both small (hillslopes) and large (fluvial) contributing areas erode significantly more than the median of the landscape.

It can seem paradoxical to argue that SS landscapes possess a time invariant erosional signature that is non-uniform across different scales, where for instance hillslopes are consistently more likely to erode than the rest of the landscape. This erosional pattern also apparently contradicts the possibility of maintaining the statistical properties of a steady state landscape, such as invariant total relief or stationary slope-area curves. The missing factor needed to reconcile these ostensible discrepancies is the dynamic character of the landforms at SS. Asserting that hillslopes are more likely to erode is not equivalent to saying that fixed locations in the landscape are more likely to erode, because individual pixels can evolve and belong to different geomorphic regimes at different times. A higher erosion rate in the hillslope pixels reduces their elevation over time and hence changes the upstream contributing areas, eventually shifting them into a regime with a lower erosion rate. To illustrate this dynamic nature of the SS topography, Fig. 3B shows that 40% of the hillslope pixels (i.e., pixels with upstream contributing areas of less than 0.5 mm^2) drain larger areas after five minutes of landscape evolution under SS (see Fig. S1 for alternative values of initial upstream area). This dynamic behavior ensures that erosion rates estimated using sediment fluxes measured at a fixed location over sufficiently long periods will converge to the erosion rate of the whole landscape, as that fixed location *visits* different regimes of the E50-area curve.

We emphasize that patterns in erosional fluxes, as shown by the E50-area curve, are easily disguised by examining the landscape in a different manner, e.g., by random sampling. For example, Fig. 3C shows the probability of erosion for pixels contained in random samples of the same size as those used to build the E50-area curve. The stationarity of the probabilities over time for fixed locations is additional evidence supporting the steady state of the landscape, and by itself might lead one to conclude that no persistent spatial patterns of erosion are expected once steady state is reached. Figure S2 shows the estimation of erosional rates when different spatial extents are considered depicting a robust behavior of those estimators for sample sizes even smaller than the one used in Fig. 3C.

The existence of time-invariant spatially-explicit patterns of erosion in SS landscapes opens questions of how to detect and characterize the response of the landscape to changing external forcing. In the next section, we show that a similar analysis reveals a significantly distinct hierarchical response of a landscape under increased rainfall intensity.

Transient State Landscape

A transient state (TS) landscape can be defined as a landscape with non-zero net material flux at the landscape scale. A TS is normally a consequence of abrupt changes in the external forcings that drive landscape evolution, such as rock uplift rate and precipitation. Using our experimental facility, we investigate the landscape reorganization at the onset of the TS that is produced by a five-fold increase in rainfall intensity. Under these conditions (*i.e.*, increasing rainfall intensity), the amount of sediment leaving the system significantly exceeds the sediment production provided by tectonic uplift:

$$\text{TS:} \quad \left\langle ED_i^{TS}\left(t,\Delta t\right)\right\rangle > U\cdot\Delta t \qquad (5)$$

Note that ED_i^{TS} depends on both t and Δt; the disequilibrium expressed in Eq. 5 gradually decays with time (17) as the landscape approaches a new SS.

We are interested in comparing the distinct dynamic response of the reorganizing landscape during the onset of TS conditions with the inherent spatial variability in erosion rates within the SS landscape. For a meaningful comparison of the sediment fluxes, however, the two landscapes must first be rendered comparable in terms of the total volume of sediment that is removed. For this, we integrate the SS and TS landscapes over different time intervals, i.e. over a longer time interval ($k\Delta t$) at SS to match the eroded sediment volume produced over an interval Δt under increased precipitation at TS:

$$\left\langle ED_i^{SS}\left(k\Delta t\right)\right\rangle = \left\langle ED_i^{TS}\left(t,\Delta t\right)\right\rangle \quad . \qquad (6)$$

Acknowledging the SS condition of Eq. 3, the time-rescaling factor k, which depends on both t and Δt, can be estimated by the volume rescaling factor, i.e., as $k = \left\langle ED_i^{TS}\left(t,\Delta t\right)\right\rangle / \left\langle ED_i^{SS}\left(\Delta t\right)\right\rangle$. Focusing our analysis on the first five minutes (*i.e.*, Δt = 5 mins) after the transition to increased precipitation rate, we found k = 2.6, meaning that an integration time of 13 mins (2.6 x 5 mins) is needed at SS to dislodge the same total volume of sediment as the first 5 minutes under TS. This ratio decreases as the integration time increases and eventually approaches k=1 at a new SS (since the uplift rate remains the same). During the experimental run, landscape topography was acquired every five minutes, and so we can only scale the SS landscape by integer values of k. By comparing the PDFs of erosion depths corresponding to different values of k (see Fig. S3), we select k=2 (i.e., topographies measured 10 min apart) in the rest of the study as the best estimate within the available temporal discretization.

The spatial patterns of erosion at TS are substantially different from those at SS (Fig. 4). To quantify the distinct distributed response occurring during the onset of the TS, we show in Fig. 5A the E50-area curves for SS (Δt = 10 mins) and for the onset of the TS (Δt = 5 mins), as well as the slope-area curve corresponding to the SS. Importantly, the E50-area curve at TS shows a significant deviation from that at SS within three distinct regions of erosional regime change under increased precipitation: (i) for areas A_i < 0.75 mm^2, there is a large percentage of high-erosion pixels for both SS and TS, but erosion is enhanced during TS compared to SS; (ii) for areas 0.75 mm^2 < A_i < 50 mm^2, the percentage of high-erosion pixels decreases with upstream drainage area in both SS and TS, but the rate of decrease is larger in TS than SS; (iii) for areas A_i > 50 mm^2, there is a regime shift from downstream-increasing to downstream-decreasing erosion: erosion increases sharply with A for SS, but for TS the fraction of highly eroding pixels decreases with A. Putting these results in the geomorphic context provided by the slope-area curve, we can conclude that during landscape reorganization in TS, hillslopes undergo accelerated erosion, colluvial and slightly convergent regions experience reduced erosion, and fluvial channels experience a reduction of their channel incision rate (erosion) due to the increase of sediment flux delivered from upstream. These results are compatible with numerical simulations by *Tucker and Slingerland* (10). It is important to note as well that the emergent scales that demarcate these erosional regime transitions coincide fairly well with the scales of geomorphic process regime transitions from hillslope to colluvial to fluvial obtained from the slope-area curve (38,44), as illustrated in Fig. 5A. To the best of our knowledge, this is the first time that such erosional regime transitions (revealed by the E50-area curves) and geomorphic process regime transitions (revealed by the slope-area curves) have been explored simultaneously at the landscape scale to detect and interpret reorganization.

This reorganization can be visualized by explicitly positioning on the landscape all pixels that transition from high to low erosion and vice versa during reorganization, relative to the landscape median erosion rate. Fig. 5B-D depicts a single drainage basin and shows the parts of the landscape that have changed their erosional behavior during the onset of TS. It is seen that hillslope pixels are the first to respond to the increased precipitation rate, shifting from low to high erosion values (Fig. 5C). In contrast, fluvial channels shift from high to low erosion values, so that incision rates are reduced due to accelerated upstream erosion and sediment supply (Fig. 5D). Although there is no distinction between sediment and bedrock in our experiment, these results resonate with recent models that suggest that sediment fluxes can exert a significant control in the river incision rates (47-50). The top-down reorganization of the landscape, with information flowing from hillslopes to channels, is distinct to the commonly-held view of landscape reorganization in response to base level changes, in which channels lead and hillslopes follow (48,51-54).

Concluding Remarks

The question of whether a steady state (SS) landscape achieves a frozen topography that exhibits no variability in local erosion rates at any scale, or achieves a statistical equilibrium within which erosion dynamically and preferentially changes locally while maintaining the large-scale balance of fluxes, remains open. Here, we analyzed a densely monitored experimental landscape to present evidence that SS is characterized by a hierarchical pattern of erosion summarized in a new curve called the E50-area curve. This curve quantifies the probability of a location eroding above or below the landscape median as a function of the location's upstream contributing area. We explained this curve in terms of the internal dynamics of the SS landscape by showing that locations of the landscape switch geomorphic regimes through time (e.g., hillslopes erode more than the landscape median, lowering their relative elevation and increasing their upstream contributing area, thus shifting to a new geomorphic regime). We proposed that the E50-area curve is a characteristic signature of SS landscapes that should be reproduced in numerical models. Finally, we showed how the shape of the E50-area curve changes when the landscape is in a transient state (TS) in response to a change in external forcing. How the shape of the E50-area curve evolves as the landscape approaches a new equilibrium in response to its forcing, and whether this new equilibrium differs from the original one, are open questions currently under experimental and analytical investigation. Extended experimental data will also allow investigation of the variability of the E50-area curve under different external forcings as an emergent property of landscape organization, informing numerical landscape evolution models and providing important information for quantifying the uncertainty of sampled erosional rates in field landscapes.

Acknowledgment:

This research was partially supported by the National Center for Earth-surface Dynamics (NCED) funded by NSF under agreement EAR-0120914 and by NSF grant EAR-1209402 under the Water Sustainability and Climate Program. A.T. acknowledges financial support from the National Center for Earth-surface Dynamics 2 (NSF grant EAR-1246761) postdoctoral fellowship. We thank Jim Mullin and Chris Ellis as well as Liam Reinhardt for helping with the development of the experimental facility (XLE). We also thank Bill Dietrich and Jean-Louis Grimaud for fruitful discussions at an early stage of this work. We would also like to thank the editor Kip Hodges, the associate editor Paul Bierman, and three anonymous reviewers for their insightful comments, which helped to improve the focus and presentation of our work.

Author contributions: All authors contributed equally to this work. **Competing interests:** The authors declare that they have no competing interests. **Data and materials availability:** All data presented in this paper can be requested from the authors.

References:

1. A. Rinaldo, W. E. Dietrich, R. Rigon, G. Vogel, I. Rodrıguez-Iturbe, Geomorphological signatures of varying climate. *Nature* **374**, 632–634 (1995).
2. K. X. Whipple, E. Kirby, S. H. Brocklehurst, Geomorphic limits to climate-induced increases in topographic relief. *Nature* **401**, 39–43 (1999).
3. A. C. Whittaker, How do landscapes record tectonics and climate? *Lithosphere* **4**(2), 160–164 (2012).
4. S. Castelltort, L. Goren, S. D. Willett, J.-D. Champagnac, F. Herman, J. Braun, River drainage patterns in the New Zealand Alps primarily controlled by plate tectonic strain. *Nature Geoscience* **5**, 744–748 (2012).
5. B. Z. Foreman, P. L. Heller, M. T. Clementz, Fluvial response to abrupt global warming at the Palaeocene/Eocene boundary. *Nature* **491**, 92–95 (2012).
6. S. D. Willett, S. W. McCoy, J. T. Perron, L. Goren, C. Y. Chen, Dynamic reorganization of river basins. *Science*, **343** (6175), 1248765 (2014).
7. S.D. Willett, M.T. Brandon, On steady states in mountain belts: *Geology*, **30**, 175–178, (2002).
8. G. Willgoose, R. L. Bras, I. Rodriguez-Iturbe, A coupled channel network growth and hillslope evolution model: 1. Theory, *Water Resour. Res.* **27**(7), 1671–1684 (1991).
9. G. E. Tucker, R. Slingerland, Drainage basin responses to climate change. *Water Resour. Res.* **33**, 2031–2047 (1997).
10. A. D. Howard, A detachment-limited model of drainage basin evolution, *Water Resour. Res.*, **30**, 2261-2285, (1994).
11. K. Stuwe, L. White, R. Brown, The influence of eroding topography on steady-state isotherms: Application to fission track analysis. *Earth Planet. Sci. Lett.*, **124**, 63–74, (1994).
12. H. Kooi, C. Beaumont, Escarpment evolution on high-elevation rifted margins: Insights derived from a surface processes model that combines diffusion, advection, and reaction. *J. Geephys. Res.*, **99**, 12,191-12,209, (1994).
13. S. D. Willett, Orogeny and orography: The effects of erosion on the structure of mountain belts, *J. Geophys. Res.*, **104**(B12), 28957–28981 (1999)
14. L. E. Hasbargen, C. Paola, Landscape instability in an experimental drainage basin. *Geology* **28** (12), pp. 1067–1070 (2000).
15. S. Bonnet, A. Crave, Landscape response to climate change: Insights from experimental modeling and implications for tectonic versus climatic uplift of topography. *Geology* **31**, 123–126 (2003).
16. A. Singh, L. Reinhardt, E. Foufoula-Georgiou, Landscape reorganization under changing climatic forcing: Results from an experimental landscape. *Water Resour. Res*. **51**, 4320-4337 (2015).
17. L. Reinhardt, M. A. Ellis, The emergence of topographic steady state in a perpetually dynamic self-organized critical landscape. *Water Resour. Res.* **51**, 4986-5003 (2015).
18. B.C. Burchfiel, M. Clark, E. Wang, Z. Chen, Y. Liu, G. Pan, Tectonic framework of the Namche Barwa region, Eastern Himalayan Syntaxis, SE Tibet, *Geol. Soc. Am. Abs. Prog.,* **32**(7), 33 (2002).
19. C.W. Naeser, N. D. Naeser, M. J. Kunk, B.A. Morgan, A.P. Schultz, S.C. Southworth, R.E. Weems, Paleozoic through Cenozoic uplift, erosion, stream capture, and deposition history in the Valley and Ridge, Blue Ridge, Piedmont, and Coastal Plain provinces of Tennessee, North Carolina, Virginia, Maryland, and District of Columbia, *Geol. Soc. Am. Abs. Prog.*, **33**(6), A312, (2001).
20. K. Sweeney, J. J. Roering, P. Almond, T. Reckling, How steady are steady-state landscapes? Using visible–near-infrared soil spectroscopy to quantify erosional variability: *Geology*, **40**, 807–810, (2012).
21. A. Densmore, M. Ellis, R. Anderson, Landsliding and the evolution of normal-fault-bounded mountains. *J. Geophys. Res.* **103**, 203–219 (1998).

22. J. D. Pelletier, Persistent drainage migration in a numerical land-scape evolution model, *Geophys. Res. Lett.* **31**, L20501 (2004).
23. L. Goren, S. D. Willett, F. Herman, J. Braun, Coupled numerical–analytical approach to landscape evolution modeling. *Earth Surf. Process. Landforms* **39**, 522-545 (2014).
24. K. L. Ferrier, K. L. Huppert, J. T. Perron, Climatic control of bedrock river incision. *Nature* **496**, 206–209 (2013).
25. J. L. Dixon, A. M. Heimsath, J. Kaste, R. Amundson, Climate-driven processes of hillslope weathering. *Geology* **37**, 975–978 (2009).
26. S. Bonnet, Shrinking and splitting of drainage basins in orogenic landscapes from the migration of the main drainage divide. *Nature Geoscience* **2**, 766–771 (2009).
27. D. W. Burbank, A. E. Blythe, J. Putkonen, B. Pratt-Sitaula, E. Gabet, M. Oskin, A. Barros, T.P. Ojha, Decoupling of erosion and precipitation in the Himalayas. *Nature* **426**, 652–655 (2003).
28. J. Han, N. M. Gasparini, J. P. L. Johnson, B. P. Murphy, Modeling the influence of rainfall gradients on discharge, bedrock erodibility, and river profile evolution, with application to the Big Island, Hawai'i. *J. Geophys. Res.* **119**, 1418–1440 (2014).
29. A. M. Heimsath, W. E. Dietrich, K. Nishiizumi, R. C. Finkel, Stochastic processes of soil production and transport: erosion rates, topo-graphic variation and cosmogenic nuclides in the Oregon Coast Range. *Earth Surf. Process. Landforms* **26**, 531–552 (2001).
30. J. D. Stock and W. E. Dietrich, Valley incision by debris flows: Evidence of a topographic signature, *Water Resour. Res.*, **39**, 1089 (2003)
31. J. J. Roering, J. Marshall, A. M. Booth, M. Mort, and Q. S. Jin, Evidence for biotic controls on topography and soil production, *Earth Planet. Sci. Lett.*, **298**, 183–190, (2010).
32. D. Lague, A. Crave, P. Davy, Laboratory experiments simulating the geomorphic response to tectonic uplift. *J. Geophys. Res.* **108**(B1), 2008 (2003).
33. K. E. Sweeney, J. J. Roering, C. Ellis, Experimental evidence for hillslope control of landscape scale. *Science* **349**, 51 (2015).
34. C. Paola, K. Straub, D. Mohrig, L. Reinhardt. The “unreasonable effectiveness” of stratigraphic and geomorphic experiments, Earth-Science Reviews, 97, 1-43 (2009)
35. D. G. A. Tarboton, A new method for the determination of flow directions and upslope areas in grid digital elevation models. *Water Resour. Res.* **33**(2), 309–319 (1997).
36. W. E. Dietrich and J. T. Perron, The search for a topographic signature of life. *Nature* **439,** 411–418 (2006).
37. A. M. Booth, J. J. Roering, and A. W. Rempel, Topographic signatures and a general transport law for deep-seated landslides in a landscape evolution model, *J. Geophys. Res. Earth Surf.*, **118**, 603–624, (2013).
38. D. R. Montgomery, E. Foufoula-Georgiou, Channel network source representation using digital elevation models. *Water Resour. Res.* **29**(12), 3925–3934 (1993).
39. A. Rinaldo, I. Rodriguez-Iturbe, R. Rigon, E. Ijjasz-Vasquez, and R. L. Bras, Self-organized fractal river networks, Phys. Rev. Lett., **70**, 822–826 (1993).
40. R. Rigon, A. Rinaldo, and I. Rodriguez-Iturbe, On landscape self-organization, *J. Geophys. Res.*, **99**(B6), 11971–11993 (1994).
41. Tucker, G.E., and R.L. Bras, Hillslope processes, drainage density, and landscape morphology, Water Resour. Res., 34, 2751-2764, 1998.
42. G. Hancock and G. Willgoose, The production of digital elevation models for experimental model landscapes, *Earth Surf. Processes Landforms*, 26, 475–490, (2001).
43. G. Hancock, and G. Willgoose, Use of a landscape simulator in the validation of the SIBERIA Catchment Evolution Model: Declining equilibrium landforms, *Water Resour. Res.*, **37**, 1981–1992, (2001).
44. D. R. Montgomery, Slope distributions, threshold hillslopes, and steady-state topography, *Am. J. Sci.* **301**, 432–454 (2001).

45. W.E. Dietrich, D. Bellugi, L. S. Sklar, J. D. Stock, A. M. Heimsath, and J. J. Roering, Geomorphic transport laws for predicting landscape form and dynamics, *in Prediction in Geomorphology*, Geophys. Monogr. Ser., vol. 135, edited by P. Wilcock and R. Iverson, pp. 103–132, AGU, Washington, D. C. (2003).
46. M. Hollander, D.A. Wolfe, E. Chicken, Nonparametric statistical methods. John Wiley & Sons. (2013).
47. L. S. Sklar, W. E. Dietrich, Sediment and rock strength controls on river incision into bedrock. *Geology*, **29**, 1087–90 (2001).
48. K. X. Whipple, G. E. Tucker, Implications of sediment-flux-dependent river incision models for landscape evolution. *J. Geophys. Res.* **107**(B2) (2002).
49. N. M. Gasparini, R. L. Bras, K. X. Whipple, Numerical modeling of non-steady-state river profile evolution using a sediment-flux-dependent incision model. In Tectonics,Climate and Landscape Evolution, WillettS, HoviusN, BrandonM, FisherD (eds). *GSA Special Paper 398, Penrose Conference Series, Geological Society of America*; 127–141 (2006).
50. N. M. Gasparini, K. X. Whipple, and R. L. Bras, Predictions of steady state and transient landscape morphology using sediment-flux-dependent river incision models, *J. Geophys. Res*., 112, F03S09 (2007).
51. A. L. Densmore, N. Hovius, Topographic fingerprints of bedrock landslides. *Geology* **28**, 371–374 (2000).
52. K. X. Whipple, G. E. Tucker, Dynamics of the stream-power river incision model: Implications for height limits of mountain ranges, landscape response timescales, and research needs. *J. Geophys. Res.* **104**(B8), 17661–17674 (1999).
53. G. E. Tucker, K. X. Whipple, Topographic outcomes predicted by stream erosion models: Sensitivity analysis and intermodel comparison. *J. Geophys. Res.* **107**(B9), 2179 (2002).
54. S. M. Mudd, D. J. Furbish, Responses of soil-mantled hillslopes to transient channel incision rates. *J. Geophys. Res.* **112**, F03S18 (2007).

Figures

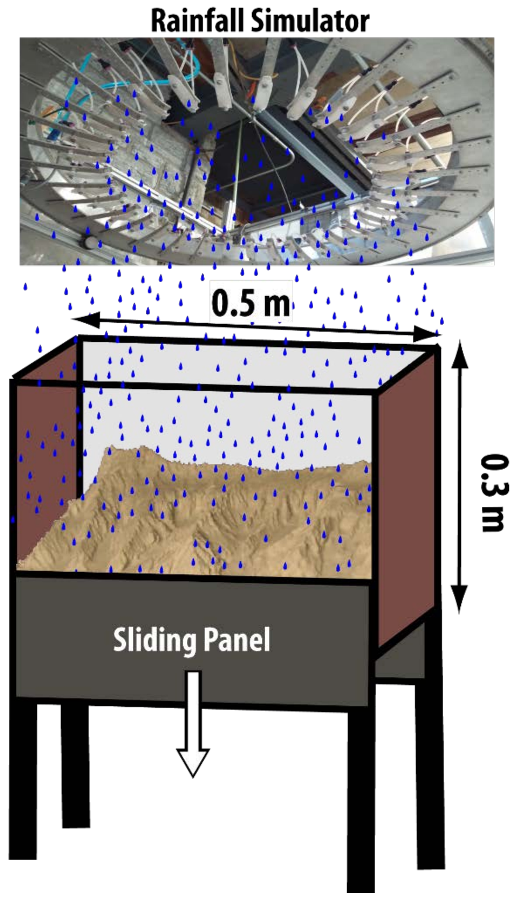

Fig. 1. Schematic representation of the eXperimental Landscape Evolution (XLE) facility at the St. Anthony Falls Laboratory, University of Minnesota.

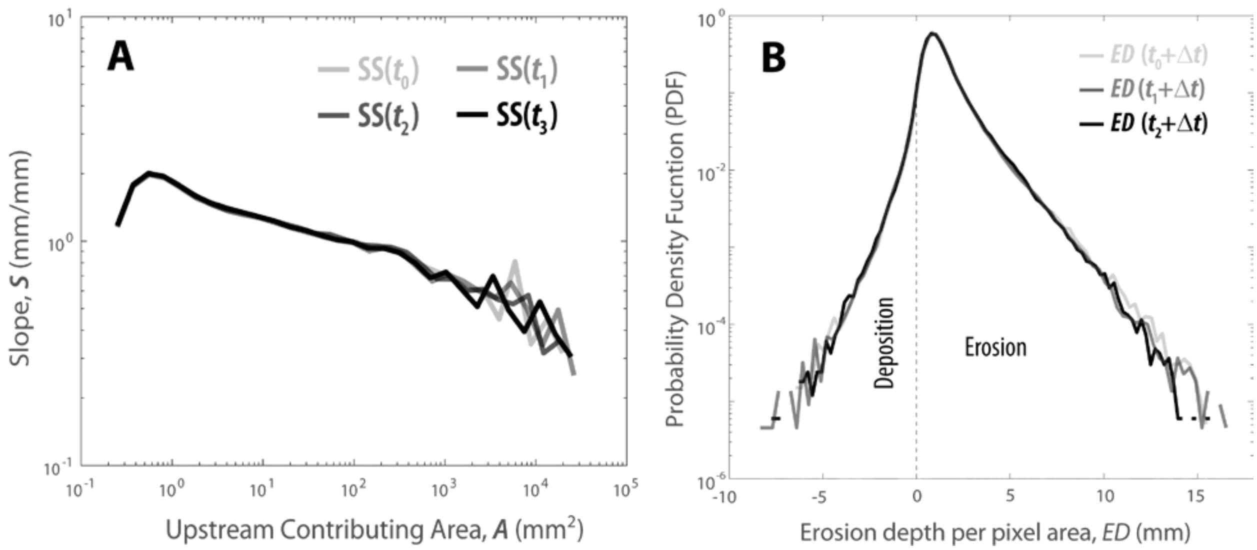

Fig. 2. Characterization of statistical steady state (SS) landscapes. (**A**) Slope-area curves of the landscape at SS computed for four different instances, separated by 5 min intervals. Note that the curves show averages over logarithmic area bins. (**B**) Probability density functions (PDFs) of the pixel-wise erosion depths computed by differencing the topographic data of the SS landscape at consecutive (5 min apart) instances. The shape of the PDF confirms the statistical nature of the SS landscape (a frozen landscape would have a Dirac delta PDF centered at the uplift depth corresponding to 5 min). The question we pose is whether every pixel of the SS landscape has equal likelihood to experience any value of this PDF (equal chance of experiencing above or below the landscape median erosion) as commonly assumed. We show that this is not the case and indeed there is a preferential scale-dependent organization of erosional fluxes as shown in Fig. 3.

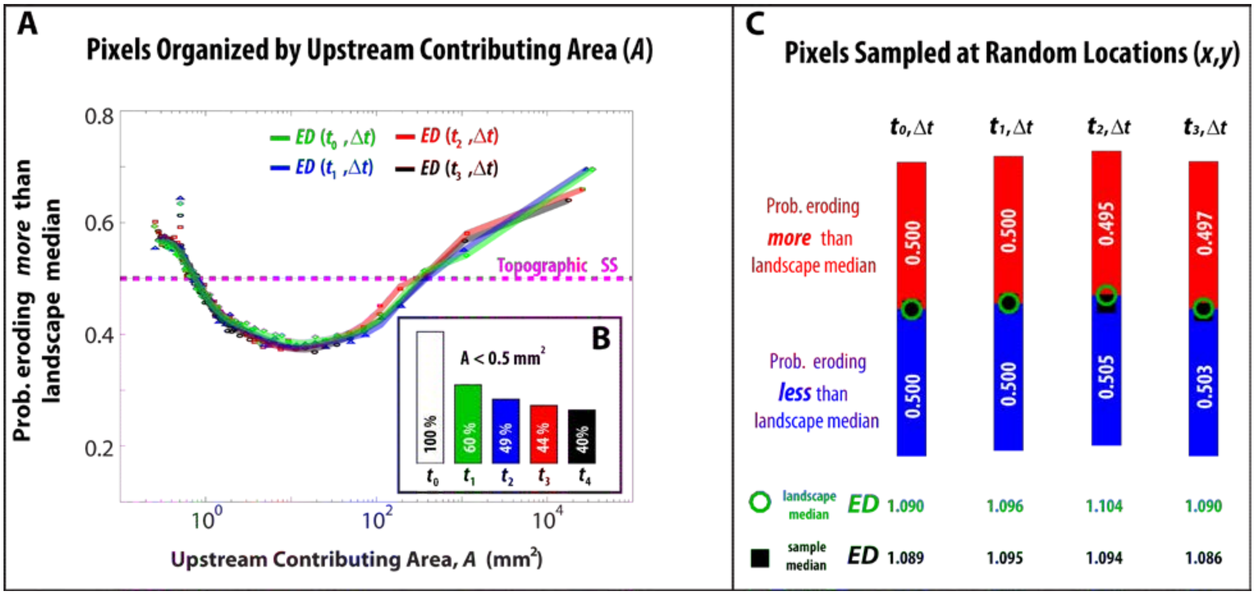

Fig. 3. Scale-dependent steady state landscape. (**A**) *E50-area curves:* The four curves (green, blue, red and black) correspond to the fraction of pixels that erode more than the landscape median plotted against upstream contributing area, *A*, and are estimated using five consecutive (5 min apart) topographies at steady state. The four curves overlap with each other, revealing a stationary statistical signature of the erosional processes acting on the landscape. The shape of E50-area curves for SS topographies clearly differs from the straight line at 0.5 probability, which would be expected either for a strict topographic (frozen) steady state landscape, or for the case where the likelihood of experiencing any value of the PDF of erosion depths is the same across the landscape. (**B**) *Dynamic landforms at SS:* The nonlinear shape of the E50-area curve shows the dynamic nature of the landforms. To illustrate the degree of their dynamic behavior, we identify at a given time (t_0) the location of all the pixels on the landscape characterized by $A < 0.5$ mm^2 (100%). For subsequent topographies acquired 5 min apart, we compute the percentage of those locations, which are still characterized by A in the same interval ($A < 0.5$mm^2). A similar analysis for different values of A is shown in Fig. S1. (**C**) *Random locations*: For a sample consisting of 1% of the landscape extent chosen randomly across the spatial domain, we examine the fraction of pixels within the sample that erode more and less than the median of the landscape over subsequent topographies. This figure evidences how the pattern revealed by the E50-area curve can be easily dismissed when spatial erosional depth patterns are interrogated in a different manner (e.g., random sampling).

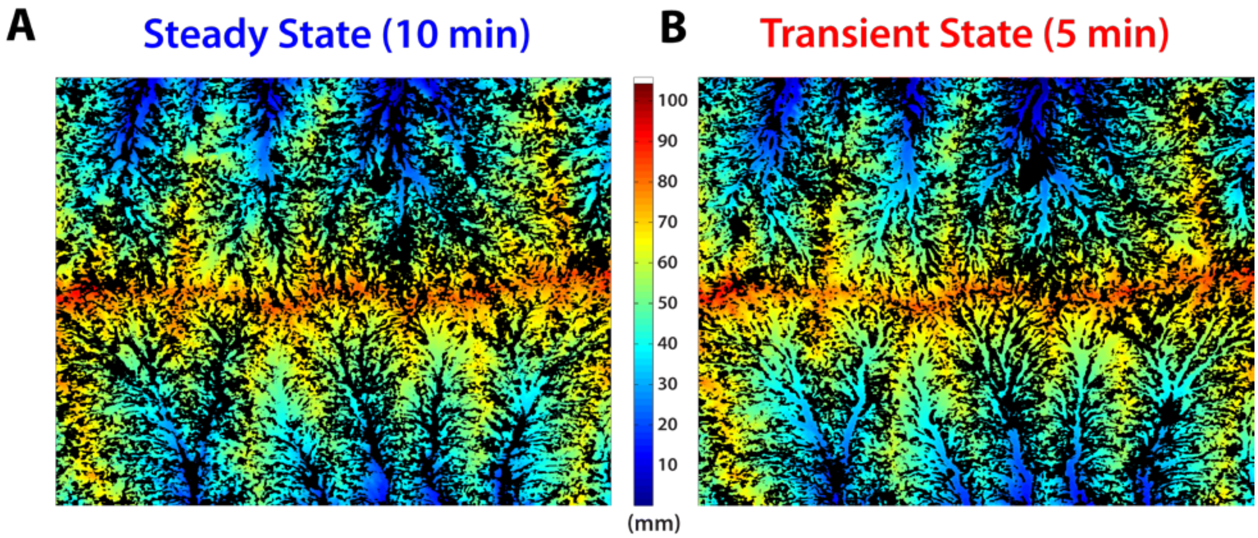

Fig. 4. Spatial patterns of erosion in steady state (SS) and transient state (TS) landscapes. Locations (black) of the highly eroding pixels (with local erosion depth above the landscape median) superimposed on the DEMs for (**A**) SS and (**B**) TS. The distinct patterns of erosion corresponding to SS and TS are apparent by visual inspection. Notice for example the lack of highly eroding pixels within the channel network at TS in comparison to SS.

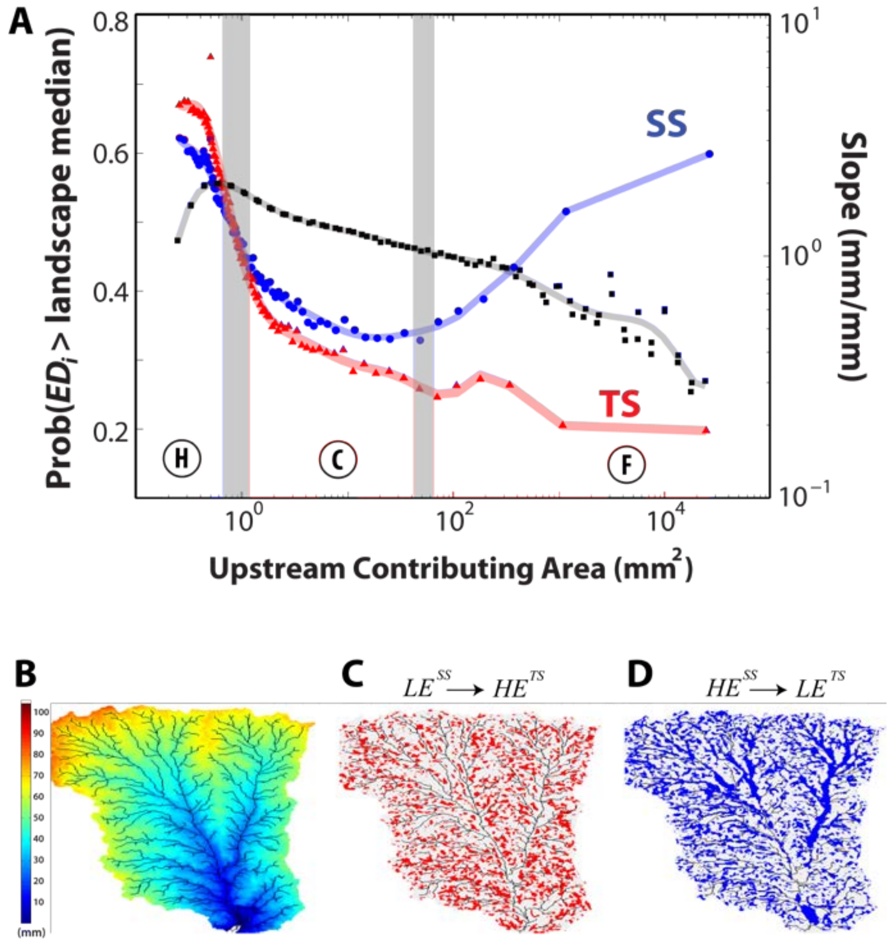

Fig. 5. Scale-dependent reorganization of the landscape. (**A**) E50-area curves for both SS (blue) and TS (red). The slope-area curve for SS (black) is also shown and the three geomorphic regimes of hillslopes (H), colluvial (C), and fluvial (F) are noted. After the onset of TS conditions, we observe increased erosion in response to increased precipitation, with this trend inverted within the colluvial regime where erosion systematically decelerates downstream. In the channels, a sediment-flux dependent incision behavior is observed, as depicted by the divergence of the E50-area curves in the fluvial part of the landscape. The vertical grey bars depict the transitions in the behavior of E50-area curves when SS and TS are compared. (**B**) DEM of a drainage basin from the experimental landscape with the river network superimposed as a reference. (**C**) Locations in the basin (red pixels) where the erosion depth has shifted from a value below the landscape median at SS (LE^{SS}) to above the landscape median at TS (HE^{TS}), showing that increased erosion occurs predominantly on hillslopes. (**D**) Locations in the basin (blue pixels) where the erosion depth has shifted from a value above the landscape median at SS (HE^{SS}) to below the landscape median at TS (LE^{TS}), showing that decreased erosion occurs predominantly within the fluvial regime.

Supplementary Material

Scale-dependent erosional patterns in steady and transient state landscapes

Alejandro Tejedor, Arvind Singh, Ilya Zaliapin, Alexander L. Densmore, Efi Foufoula-Georgiou

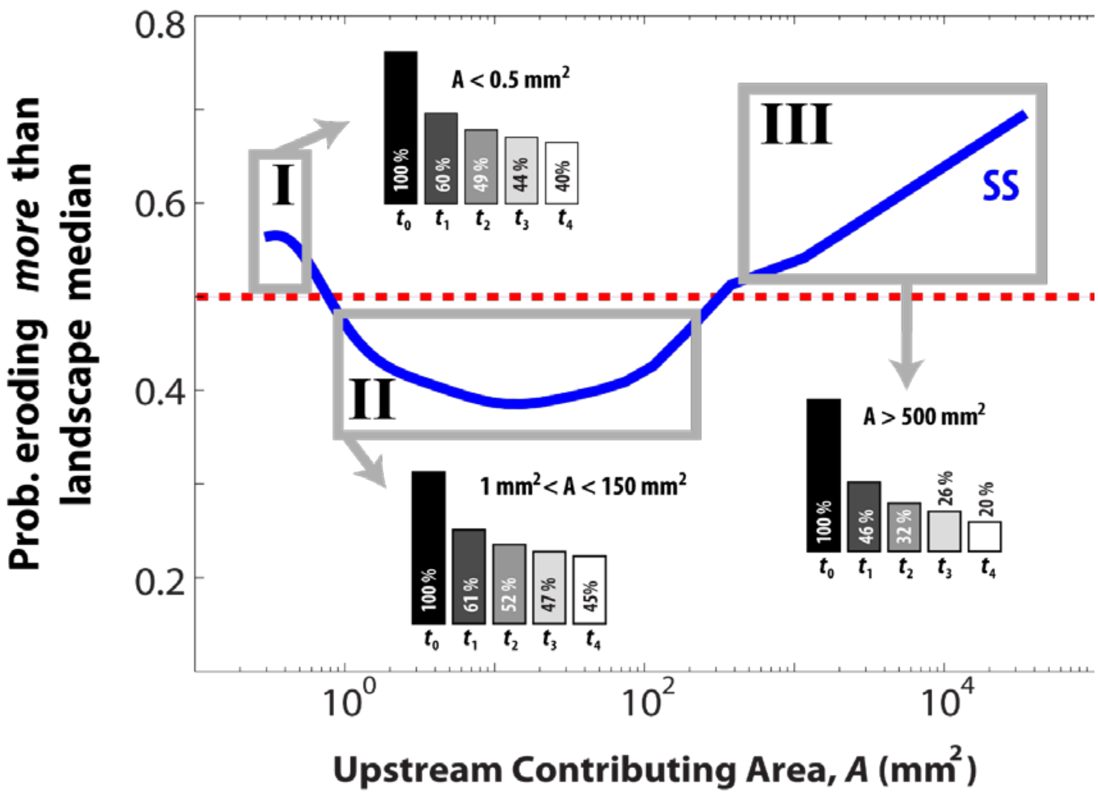

Fig. S1. Dynamic Landforms at Steady State. The shape of the E50-area curve reveals that the likelihood of eroding more (or less) than the median of the landscape is nonlinearly related to the upstream contributing area, *A*. We examine the dynamic nature of steady-state landscapes within three ranges of upstream contributing areas: (**I**) $A < 0.5 mm^2$, with a higher likelihood of eroding more than the median of the landscape; (**II**) $1 mm^2 < A < 150 mm^2$, with a lower likelihood of eroding more than the landscape median; (**III**) $A > 500 mm^2$, with a higher likelihood of eroding more than the landscape median. We identify at a given time (t_0) the location of all the pixels on the landscape within each of the three ranges defined above (100%). For each subsequent topography (measured 5 min apart), we compute the percentage of pixels on those locations, which are still characterized by *A* in the same interval as initially defined. The inset plots show that, in each area range, a significant percentage of pixels change their upstream contributing areas over time, illustrating the dynamic nature of steady-state landscapes.

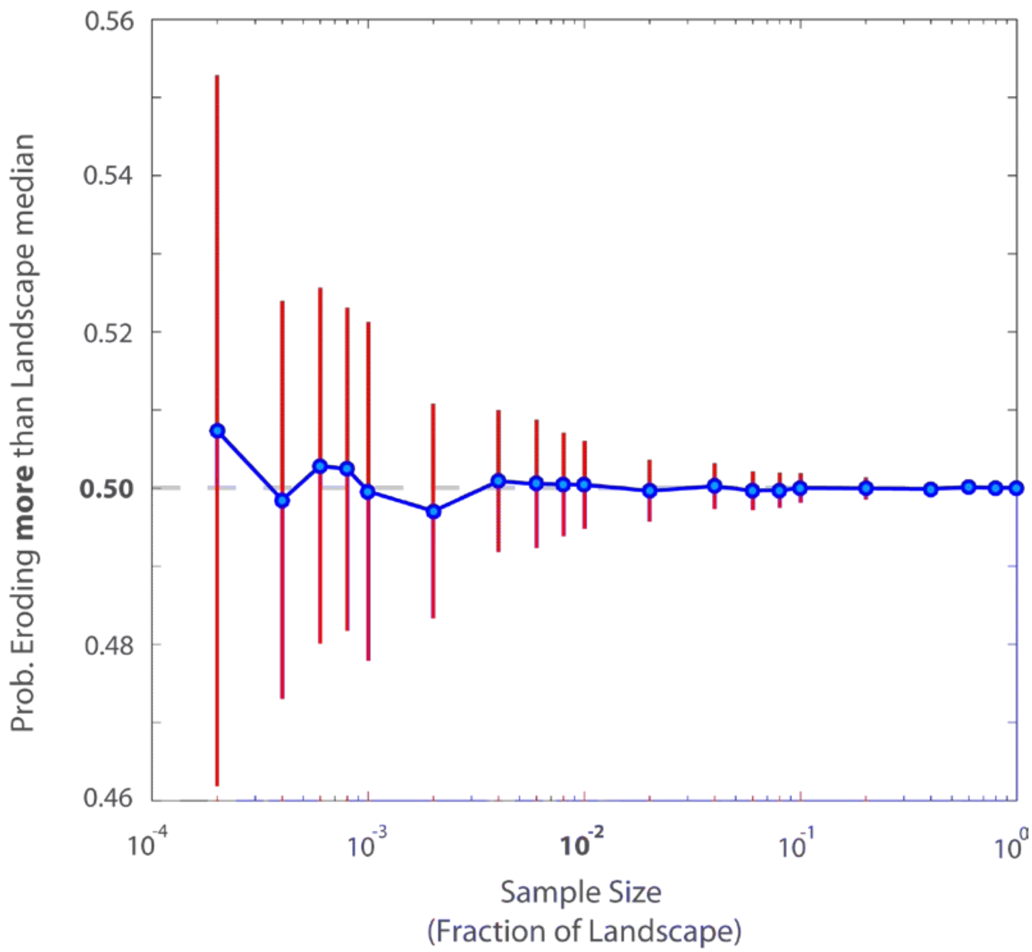

Fig. S2. Estimation of the probability of erosion larger than the landscape median at SS for different sample sizes. Blue circles correspond to the estimated probability of eroding more than the median of the landscape (Y axis) by using 100 randomly selected samples of a given size (X axis). The red lines correspond to standard deviations estimated from the 100 samples. Note that to construct the E50-area curve we used 100 bins, which have a constant sample size equal to 0.01 fraction of the landscape. From the results corresponding to sample size equal to 10^{-2} shown in this figure, we can conclude that the patterns depicted by the E50-area curves (see Fig. 3 and 4 in the main text) are statistically significant.

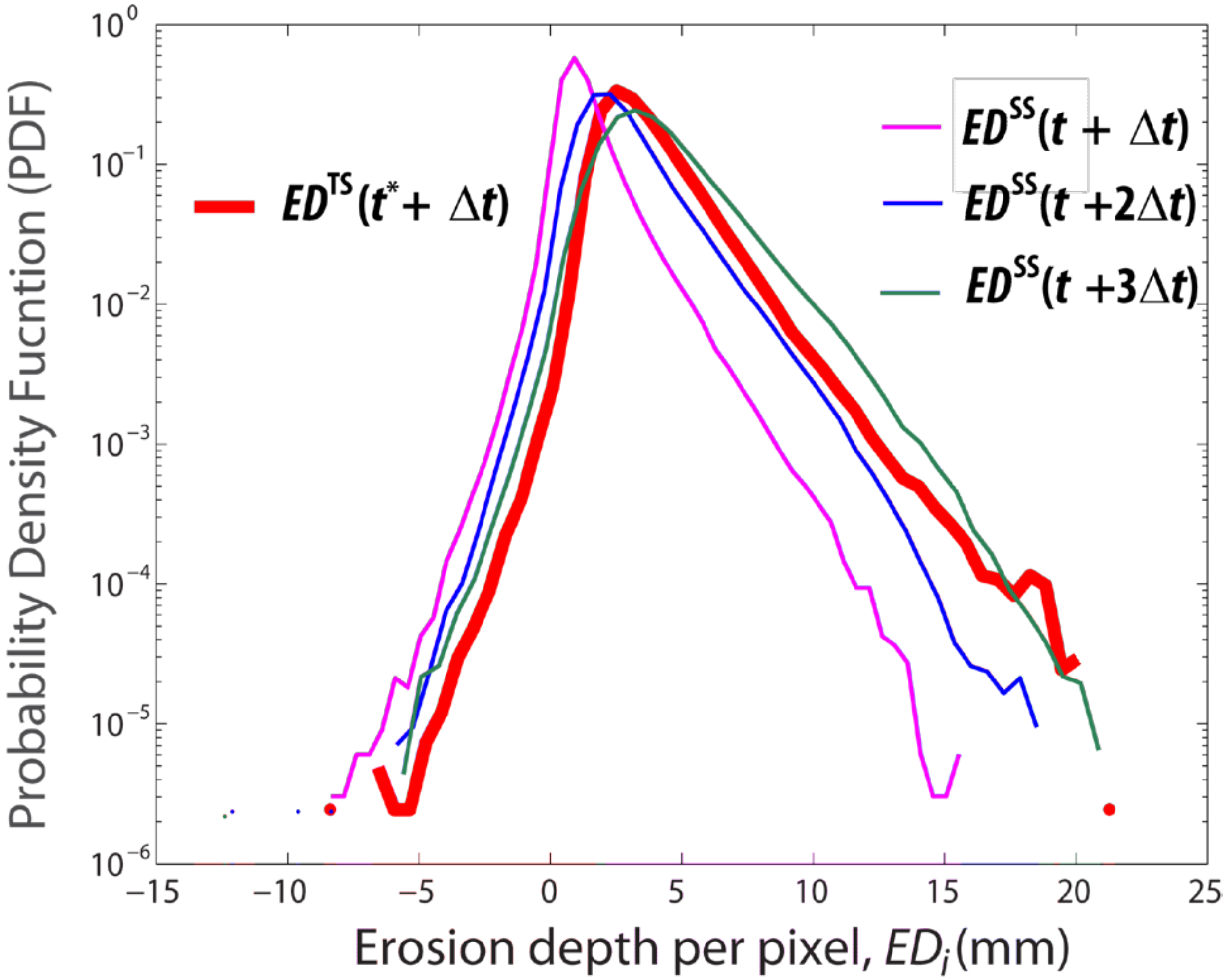

Fig. S3. Comparison of the steady-state (SS) and transient-state (TS) landscapes in terms of the aggregate statistics of erosion depth. Probability density functions (PDFs) of erosion depth per pixel, ED_i, in the TS landscape, subject to a five-fold increase in precipitation intensity during 5 minutes (Δt) starting at time t* (red curve), and the SS landscape during 5 (magenta), 10 (blue), and 15 (green) minutes.